UCL CoMPLEX Case Presentation 3:

Global imaging of cancer in live zebrafish using optical projection tomography

Author: Matthew Topping

Supervisors: Dr. Paul Frankel
Dr. Matilda Katan-Muller

Abstract

It is of the utmost importance, considering the substantial present and projected future global burden of cancer, that new treatments of cancer are developed and system models are improved. Zebrafish are for many reasons an excellent model to use, not least because of the ease of use they allow for using imaging techniques such as the fluorescence labelling of cells of interest. In order to investigate tumour progression in a novel inducible zebrafish tumour model a longitudinal study of six zebrafish was performed. Upon induction of tumour formation Optical Projection Tomography was conducted to image the fish. The images were then reconstructed via a filtered back-projection algorithm and tumour progression and vascularisation was investigated for each fish. Significant tumour progression was observed in two zebrafish followed across three imaging rounds. Simultaneously, biosensors intended for use in this zebrafish genetic cancer model were first verified and then used to transfect cells to study their expression. Finally the Maximum Tolerated Dose of doxycycline for the zebrafish was examined, with outcomes suggesting the use of a reduced concentration should be investigated. The results of this report demonstrate the effectiveness of OPT techniques and propose future improvements that could be made.

Contents

List of figures

List of tables

Introduction

Cancer is one of the primary causes of mortality and morbidity worldwide with an estimated 7.6 million deaths being caused by the disease in 2008 alone [WHO, 2013]; this figure is projected to increase to 13.1 million by 2030 [WHO, 2013] which is partly the result of an increase in the proportion of the population that is elderly, who are known to be the group most susceptible to cancer [Yancik and Ries, 2004]. It is therefore clear that despite huge advancements and successes in the field of cancer treatment over the past few decades [Richards *et al*., 2000] an even greater effort will be required in the future if those mortality figures are to be reduced, particularly with regards to models of cancer initiation and progression.

Although traditional cancer models have tended to be murine or *Drosophila* based, in the recent past this has changed somewhat as the zebrafish (*Danio rerio*) has emerged as one of the most popular model animal systems. This is at least partly because the small size of the zebrafish allows for the use of fluorescent imaging techniques such as Förster Resonance Energy Transfer - Fluorescence-lifetime Imaging Microscopy (FRET-FLIM), meaning that the development of tumours can be studied over larger timescales. This is of particular significance considering the importance of live disease model investigations because of the potentially large differences between biological processes that occur *in vivo* as opposed to *in vitro* - for example, a recent review of cancer hallmarks [Hanahan and Weinberg, 2011] identified a number of attributes, such as angiogenesis induction and invasion activation, which must be studied *in vivo.*

Unfortunately, zebrafish tend to quickly grow to the point where conventional confocal microscopes are no longer able to image the whole animal. Recently however Optical Projection Tomography (OPT) has been used in an increasingly large variety of studies and it has been shown that it can be utilised to image live zebrafish older than 30 days post fertilization [McGinty *et al.*, 2011].

With this in mind, this project focused on conducting a longitudinal study of tumour growth in six zebrafish in order to study not only the amount of tumour progression but also the interface between the surrounding vasculature and the tumour itself. Tumours were induced in the zebrafish using the Tet-on-Ras system, and the fish were then imaged twice a week over the next 2 weeks. Alongside the imaging segment of the project, several biosensors which will be used in future studies were verified for correct sequence identity and checked for correct expression. The Maximum Tolerated Dose (MTD) of the genetic inducer, Doxycycline, was also investigated to explore the relative amount of tumour progression possible, with results suggesting that using a reduced concentration compared to the standard concentration currently used could be advantageous. The images reconstructed indicate not only the significant level of tumour progression but also the potential of OPT for longitudinal studies of tumour growth.

Background

Rationale behind model choice

Zebrafish models of cancer are becoming increasingly popular of late because of a large number of advantages, including relative cost effectiveness [Allen and Neely, 2010], huge brood sizes [Feitsma and Cuppen, 2008] and the availability of transparent casper mutant zebrafish that are continuously transparent until death [Stoletov and Klemke, 2008].

In addition to this, tumours that have developed in zebrafish share large similarities with those that formed in humans [Amatruda *et al*., 2002] (especially for tumours formed as the result of pancreatic cancer [Davison *et al.*, 2008], amongst others), allowing for the creation of accurate zebrafish models of human cancers [Liu and Leach, 2011]. Indeed it is estimated that nearly 70% of disease genes in humans are present in some manner in zebrafish [Langheinrich, 2003], indicating that despite some unfortunate disadvantages (namely the inability to construct lung and mammalian

gland cancer models for obvious reasons [Santoriello and Zon, 2012]) it remains an extremely viable model.

Of specific relevance to this project are zebrafish models of liver tumourigenesis, a number of which have been developed and proposed for use as a cancer therapy screening platform [Nguyen *et al.*, 2012]. Such models have been utilised to investigate the role of various different molecules in this process, such as the fish oncogene *xmrk* [Li *et al.*, 2012] and the transcription factor *Myc* [Li *et al.*, 2012a], and represent a growing area of study.

Rationale behind imaging technique choice

FRET involves the radiationless donation of energy from one fluorophore (denoted the 'donor') to another in the close vicinity (denoted the 'acceptor'), provided that the emission spectrum of the donor contains at least part of the absorption spectrum of the acceptor. FRET takes places over incredibly short distances, with the transfer efficiency decreasing according to the sixth power of the distance between the two fluorophores [Zheng, 2006]. This incredible sensitivity means that FRET efficiency can be utilised as an excellent measure of the proximity of the two fluorophores, particularly when the two molecules are attached to the same probe.

The efficiency can be measured by using FLIM, because the transfer of energy from the donor to the acceptor leads to a shorter donor fluorescence lifetime than would otherwise be expected [Chang *et al.*, 2007]. FLIM has the major benefit of ignoring the concentrations of the various fluorophores as intensity is not important in this case. FRET-FLIM techniques therefore provide a suitable method for exploring a variety of cell processes such as protein diffusion [Verveer and Bastiaens, 2007] or, as in the case of this project, tumour development. In this instance OPT was chosen to be used as the method of object volume reconstruction.

OPT allows for the reconstruction of a 3D image using back projection algorithms by taking a large number of pictures of the desired object from different angles using light microscopy. By using a significant field depth when taking the pictures it is possible to accurately image objects between 1 and 15 mm without needing to damage the object [Sharpe *et al.*, 2002], meaning that it can be utilised for specimens that are too small to be suitable for Magnetic Resonance Imaging but too big for confocal microscopy [Sharpe, 2004]. In addition to these advantages, it has only a moderate associated cost [Spitsbergen, 2007] and as such variants of OPT are frequently used for imaging samples such as zebrafish [Bassi *et al.*, 2011; Fieramonti *et al.*, 2012]. The method is continually improving as a means of investigation, with major improvements in motion correction and sample alignment being made recently [Cheddad *et al.*, 2012; Zhu *et al.*, 2012].

FRET-FLIM techniques used in tandem with OPT can produce clear and defined pictures of living biological systems [McGinty *et al.*, 2011] and as such were ideally suited for the project.

Biosensors

The biosensors chosen for use in this project were designed to study the activity in cells of three different molecules that are known to be involved in the development of cancer: Membrane type 1 matrix metalloproteinase (MT1-MMP), Rac and Src kinase. MT1-MMP is strongly thought to be involved in cancer cell malignancy and angiogenesis [Seiki, 2003; Seiki *et al.*, 2003], whilst Rac is a small GTPase with a role in modulating cell protrusion and the formation of lamellipodia [Hall, 2005]. Finally, Src kinase plays a vital role in determining the invasive ability of cancers [Ishizawar and Parsons, 2004] and has been demonstrated to interact with, and regulate, both MT1-MMP [Nyalendo *et al.*, 2007] and Rac [Ouyang *et al.*, 2008]. It is not yet clear however exactly how the temporal and spatial activities of these three molecules have an impact on cancer progression.

The three biosensors contained different fluorophores in order to prevent problems occurring because of unwanted overlapping emission/absorption spectrums, and their development is described in detail in previous papers [Ouyang *et al.*, 2010; Ouyang *et al.*, 2008]. Briefly, the MT1-

MMP biosensor consisted of a mCherry and mOrange2 (chosen because of a much larger photostability than regular mOrange) pair connected with a substrate peptide sequence and then fused with a platelet-derived growth factor receptor via the receptors transmembrane domain, with the Rac biosensor being comprised of CFP and YPet (an alternative yellow fluorescent protein) linked to Rac1 and PAK1. The Src biosensor contained ECFP and Citrine and was created by joining a KRas prenylation substrate sequence to the COOH end of one of the fluorophores. The biosensors were then cloned into expression vectors sourced from inVitrogen™, with the MT1-MMP and Src biosensors being inserted into the vectors pDisplay™ and pcDNA™ 3.1 respectively [Invitrogen™, 2010; Invitrogen™, 2010a]. The MT1-MMP and Src biosensors were obtained from Sean Warren, whilst the Rac biosensor was already available. As an example, a visual representation of the mechanism of action for the Src biosensor is provided in Appendix I.

These biosensors have been used previously to investigate the hierarchical relationships between Src and Rac [Ouyang *et al.*, 2008] and to observe in living cells Src and MT1-MMP molecular activity [Ouyang *et al.*, 2010], particularly with regards to MT1-MMP spatiotemporal regulation [Ouyang *et al.*, 2008a] and are planned for use in future zebrafish cancer model studies.

Aims

The project was split into two separate, but complimentary, parts: one used *in vitro* experiments to examine biosensor expression whilst the other utilised *in vivo* imaging techniques to capture tumour growth in zebrafish.

The major aim of the first section was to ensure that the biosensors selected showed a reasonable level of expression in the expected place in the cell and to judge whether they were suitable for the construction of cell lines involved in xenograph production. These *in vivo* experiments were quicker, with first a transient transfection being conducted to check if expression occurred at all before a stable transfection was undertaken to look more precisely at expression in two different cell types.

The second section by contrast investigated the progression of induced tumours in zebrafish over the course of two weeks, with the main aim of exploring the growth of the tumours and the tumour vascularisation that occurred as a result. The fluorophores GFP and mCherry were chosen as markers for the tumour and the vasculature respectively because of their reliability and lack of cross-reactivity.

Materials and methods

Sequencing of biosensor constructs

In order to ensure that the MT1-MMP and Src biosensors utilised were in fact the correct biosensors to use, they were first sent for sequencing by Source Bioscience (http://www.lifesciences.sourcebioscience.com/genomic-services/sanger-sequencing-service.aspx): this was not necessary for the Rac biosensor as this was already a known quantity. Two rounds of sequencing were conducted, with the first using primers taken from the inVitrogen™ website for each end of the biosensor sequence. Whilst this was found to be sufficient to create a complete sequence for the MT1-MMP biosensor, the results for the Src biosensor were found to be inadequate. Thus a second round of sequencing was done for the Src biosensor only, with three different primers created using an online sequencing programme (http://www.ncbi.nlm.nih.gov/tools/primer-blast/) and the already known segments of the sequence. All three primers were between 20 and 21 base pairs long, and were selected such that the melting temperature was between 50 and 60 °C and the primers contained a minimal amount of self-complementarity. This resulted in enough information to create a complete sequence for the Src biosensor.

Information provided in the description of the development of the biosensors was used to

help correctly identify the biosensors [Ouyang *et al.*, 2010] by providing a rough idea of the sequence, before online tools were used to first translate the nucleotide sequence to a protein sequence (http://web.expasy.org/translate/) and then search known protein databases for matches (http://blast.ncbi.nlm.nih.gov/Blast.cgi).

Cell maintenance

Two different transfections were undertaken during the experiment; one transient, the other stable. For both transfections, 5 x 10^5 cells were seeded into the single wells of a six well plate and allowed to grow to over 80% confluency overnight. In both cases, they were transfected the next day according to the appropriate protocol, with transient transfections using Lipofectamine™ 2000 (Invtrogen®, 2012) and stable transfections using FuGene® (Roche, 2013) – the protocols followed for the different transfection types are available in the reference section. For the transient transfection the cell line used was Human Embryonic Kidney (HEK) 293 cells, whilst U87 and U251 brain tumour cells were utilised for the stable transfection.

Zebrafish selection and maintenance

Six casper mutant zebrafish were selected at the start of the study with the preferred, but not necessary, selection condition of the fish all being a similar size. Their weights were measured partway through the experiment and are given in table I in the results section. The values given indicate that the criterion was not fulfilled, but this does not pose a significant concern. The fish were all born 56 days before the experiment began and all fish were maintained in compliance with conventional guidelines. Their water was changed every day and they were fed with a standard feed which included krill and shrimp. Doxycycline was used as the genetic inducer and was replaced every other day, with a standard concentration of 15 mg/L being used.

Experimental set-up

All OPT imaging took place in the Physics department of Imperial College London with the assistance of Lingling Chen and Sunil Kumar. In terms of experimental schematics, the set-up of the OPT system is similar to that of a microscope system. The zebrafish were placed under a rotation stage (purchased from Newport Corp) and were held in a setting that was refractive-index matched. The wide-field excitation was created by a commercially available ultrafast fibre-laser-pumped super-continuum light source (SC400, Fianium Ltd.) and images of the different fish were taken using a suitable chromatic emission filter in conjunction with a tube lens combination onto a charge-coupled device camera.

Before being imaged, the fish were exposed for two and a half minutes to a 100% tricaine solution in order to induce anaesthesia. The length of time and anaesthesia concentration were chosen based on previous experiments [Huang *et al.*, 2010] As this was found to be insufficient for some of the larger fish, the time spent in the anaesthetic was increased to approximately four minutes for these fish. Unfortunately the uncertainty over the length of time needed to anaesthetize the fish led to the death of two of the larger fish. Whilst being imaged the zebrafish were placed into a short piece of sealable translucent tubing containing a 50% tricaine solution, which was itself held in place in a container full of cold water, in order to maintain and prolong the unconsciousness of the fish [Wilson *et al.*, 2009].

Image reconstruction

The 3-D images were reconstructed by the use of a back-projection algorithm similar to that explained in previous works [Kak and Slaney, 1988]. A more comprehensive description of the theory behind OPT is available in other works [McGinty *et al.*, 2011], but in brief the pixel rows of

a captured image are thought of as 1-dimensional projection of a 2-dimensional segment of the object being imaged. By rotating the sample around its axis a sinogram is formed from these projections, which allows for reconstruction of the entire signal by utilising an inverse Radon transform. This transform first Fourier transforms the projection, filters the results and then inverse Fourier transforms this filtered data and is repeated for all projections available, allowing for a 3-D image to be formed.

Results and discussion

Biosensor component

Verification of biosensors

The biosensors that were sequenced were confirmed as being as expected using the techniques outlined previously. The nucleotide and protein sequences for both the MT1-MMP and Src biosensors are given in Appendix I, along with images displaying the various regions of the biosensors.

In addition to the sequencing that was conducted, a western blot of HEK 293 cells that had been transfected with various constructs was performed following a set standard protocol. Biosensors for GFP, mCherry, MT1-MMP and Src were used as probes with the results for the GFP biosensor shown in figure I seen below. The results for the other biosensors were not included because they were rendered unnecessary by the results of the GFP biosensor, which produced a much clearer blot than the others – in particular the MT1-MMP biosensor produced a blot of especially poor quality.

Clearly from the results one can identify GFP as being present in the correct place each of the expected lanes (as it obviously should not be present in the untreated lane), providing further proof that the MT1-MMP and Src biosensors were correctly identified.

Transient transfection results

In order to investigate whether the transient transfections had been successful and that the biosensors were behaving as expected, fluorescence microscopy of cells containing the biosensors was conducted. From the images displayed in figure I it can been seen that both MT1-MMP and Src transfected cells exhibit clear membrane staining, which is in line with expectations: the MT1-MMP biosensor should contain a platelet-derived growth factor receptor which is situated outside of the plasma membrane whilst the Src biosensor should be attached to the membranes inner side. This membrane staining is not as clear for the Rac biosensor because it does not contain a membrane associated domain.

a)

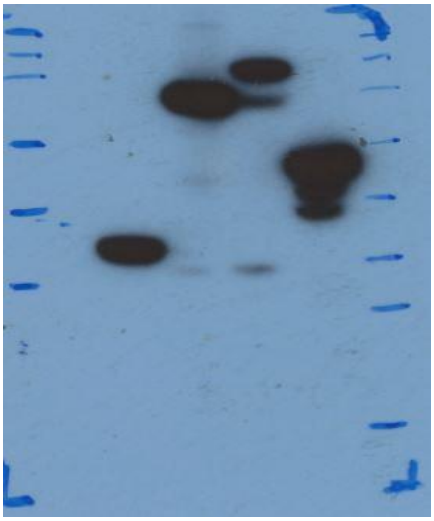

b)

c)

d)

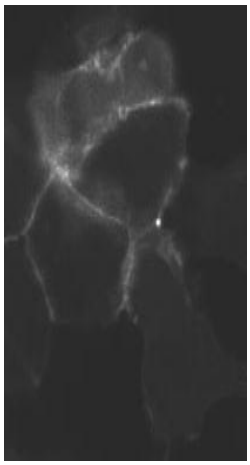

Figure I: a) shows the results of a Western Blot performed using the GFP biosensor mentioned above. The five lanes present in the results characterise each of the five types of sample investigated: they represent proteins taken from cells that were treated with nothing, mCherry and GFP, MT1-MMP, Src and Rac respectively. The numbers on the right hand side represent the length in kDa of the proteins. b), c) and d) represent fluorescence microscope images of transiently transfected cells containing the MT1-MMP, Rac and Src biosensors respectively.

Stable transfection results

After the transient transfections were shown to be successful, stable transfections were conducted to further investigate the biosensors. Unfortunately there was insufficient time during the project for large cell colonies to form, meaning that the images are not as ideal as might be hoped to demonstrate successful transfections – there was also inadequate time to perform a Western Blot, which could have help to verify if the transfections were fruitful. However, they do indicate that at least some cells were transfected correctly for all three biosensors.

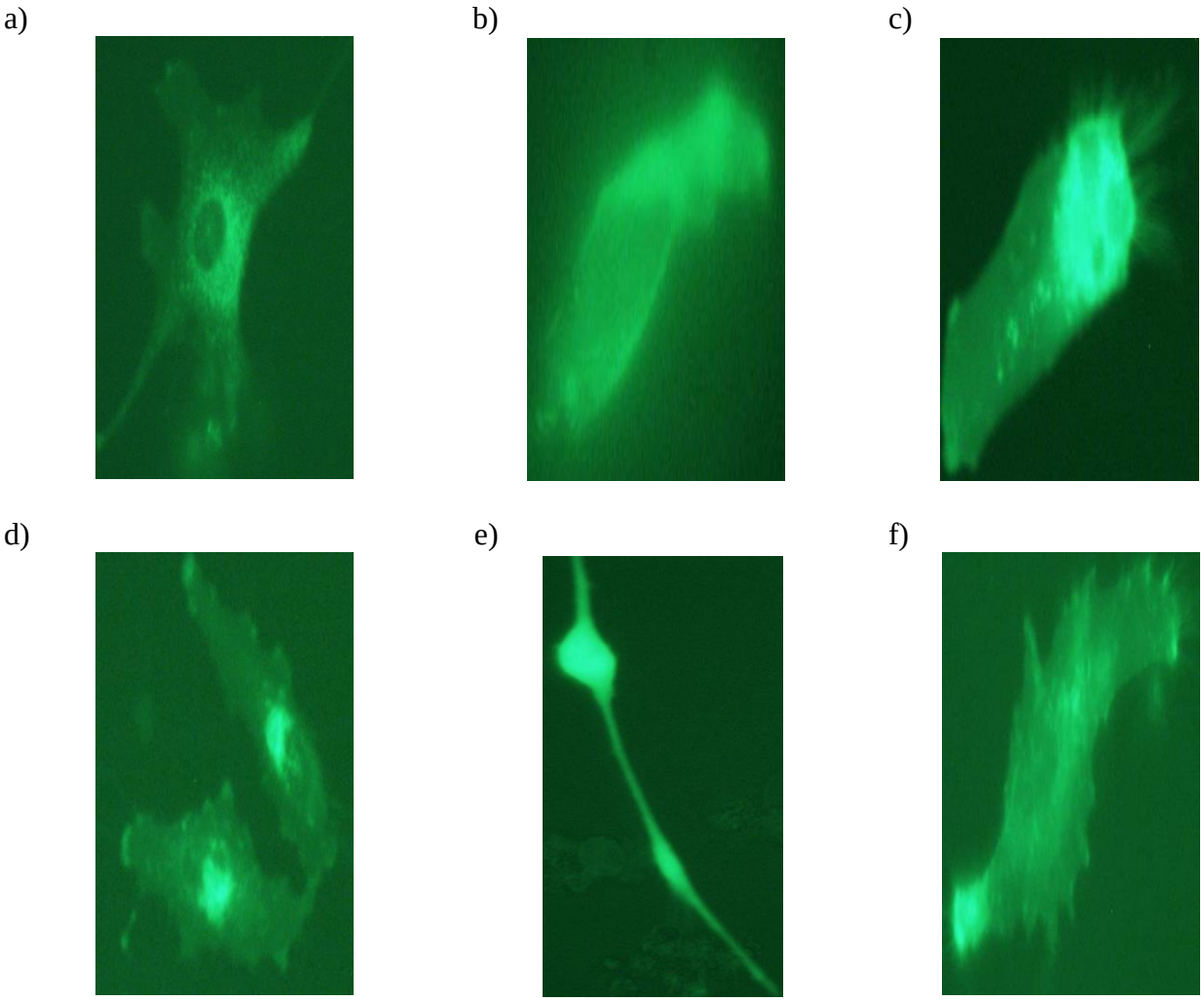

Figure II: Fluorescence microscope images of stably transfected U87 cells containing the a) MT1-MMP, b) Rac and c) Src biosensors respectively and of stably transfected U251 cells containing the d) MT1-MMP, e) Rac and f) Src biosensors respectively

Zebrafish component

Zebrafish imaging prior to tumour inducement

Fluorescent images of each zebrafish were taken using confocal microscopy before tumour inducement was commenced to investigate the level of auto-fluorescence occurring in the animals.

a) b)

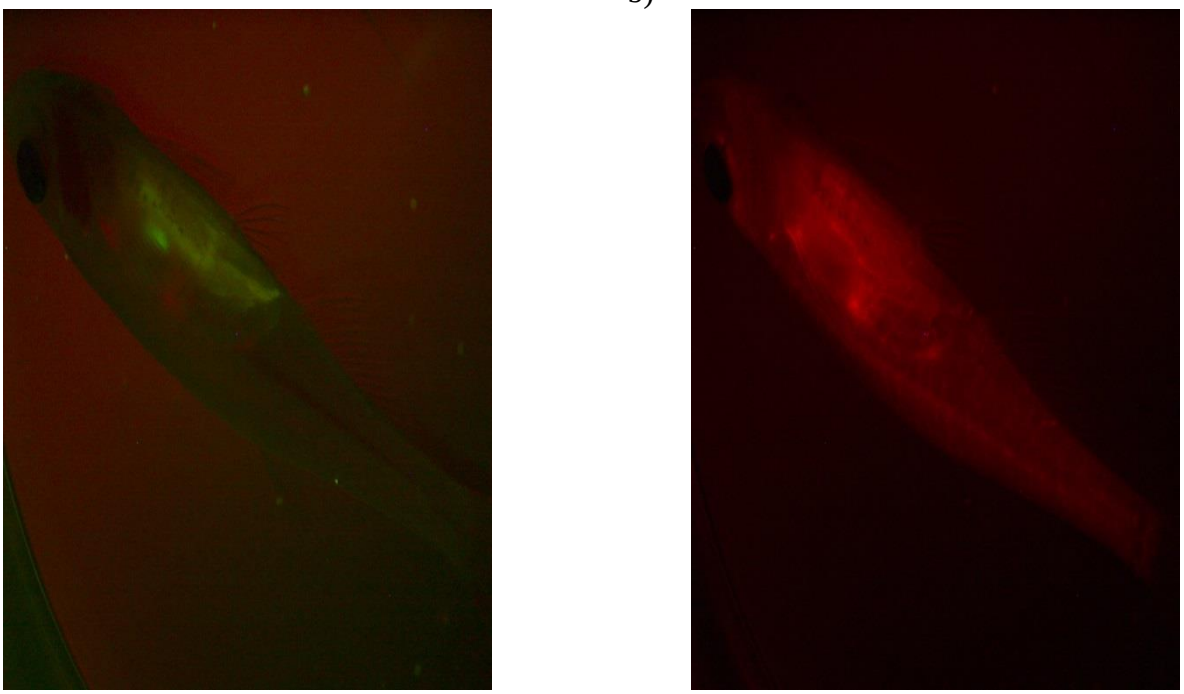

Figure III: Fluorescence microscope images of fish 1 with respect to a) GFP and b) mCherry

The figure above shows the amount of auto-fluorescence, which is particularly important on the red and green channels considering the use of GFP and mCherry in this experiment, occurring in a representative zebrafish. There is clearly some auto-fluorescence taking place, but not at a significantly high level as to interfere with experiment.

Changes in zebrafish weight throughout study

Zebrafish weight can be used as a marker of tumour growth, although it should be noted that changes in weight may not solely be due to tumour growth as large amounts of fluid associated with tumour formation can also be produced.

The fish were first weighed one week after being first introduced to water containing doxycycline, and then weighed again another four and finally seven days later (i.e. eleven and fourteen days into the experiment respectively). By the time of the final weighing all the zebrafish had died with the exception of fish 6, which died shortly afterwards.

Fish number	Weight at first weighing (mg)	Weight at second weighing (mg)	Weight at third weighing (mg)
1	280	460	Deceased
2	200	Deceased	Deceased
3	360	Deceased	Deceased
4	290	Deceased	Deceased
5	440	620	Deceased
6	120	230	210

Table I: The weight in milligrams of the six zebrafish selected for imaging, taken at various points throughout the study.

From the table above it is obvious that tumour progression was significant with one fish almost doubling in weight between the two measurements (although half the fish did not even survive long enough for a second weighing). As such the death of all of the fish is not surprising, particularly when the traumas associated with transportation and regaining consciousness after being anaesthetized are accounted for. The latter ordeal becomes progressively more difficult as the tumour continues to grow, meaning that the zebrafish become increasingly likely to never recover consciousness as the tumour progresses. There is also the possibility that the doxycycline concentration used was in fact toxic to the fish, as several of the fish died between rounds of imaging after successfully surviving both the anaesthetic and transport.

Images of tumour progression

As can be seen from Table III, only two fish survived long enough for more than two sets of images to be obtained, although two full rounds of imaging were completed.

Fish number	Imaging round I: experiment day 4	Imaging round II: experiment day 7	Imaging round III: experiment day 11	Imaging round IV: experiment day 14
1	✓	✓	✓	×
2	✓	✓	×	×
3	✓	✓	×	×
4	✓	✓	×	×
5	✓	✓	×	×
6	✓	✓	✓	✓

Table II: The date and identity of each fish that was included in each round of imaging

Figure IV below contains images showing the changes in tumour size and vasculature structure over the course of the imaging for fish 1 – figure III contains images of the same fish prior to tumour inducement. Gifs of the image sequences are included in appendix III.

a)

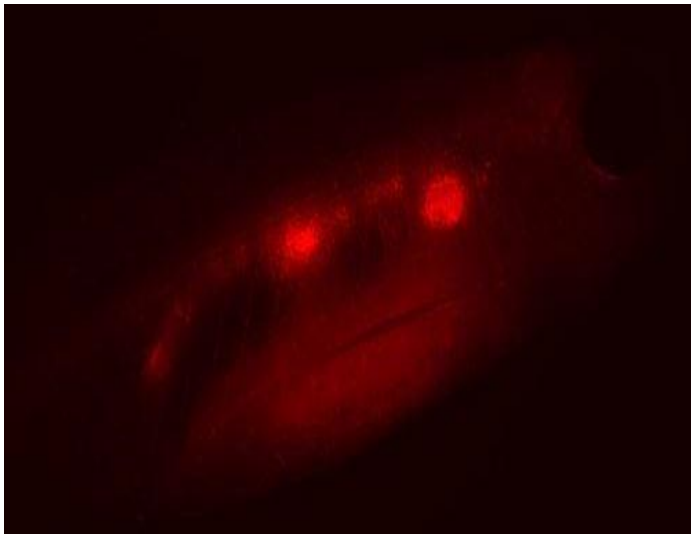

b)

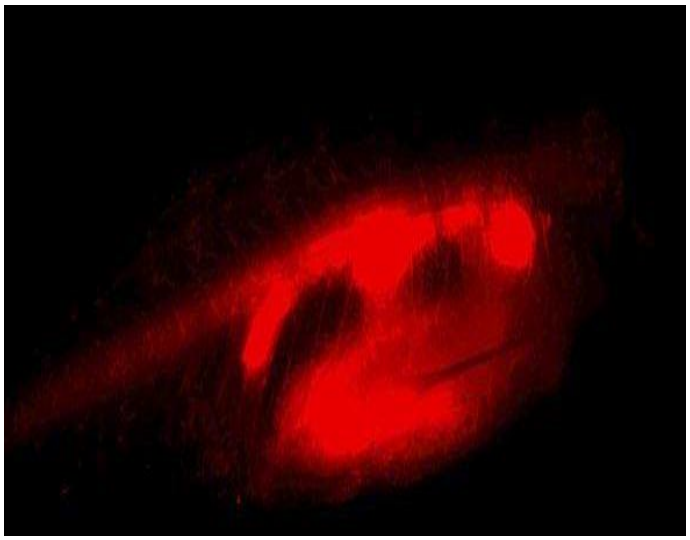

c)

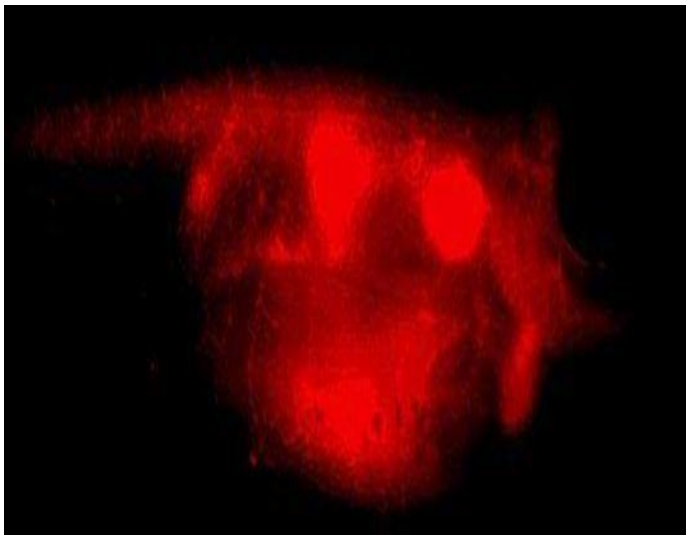

d)

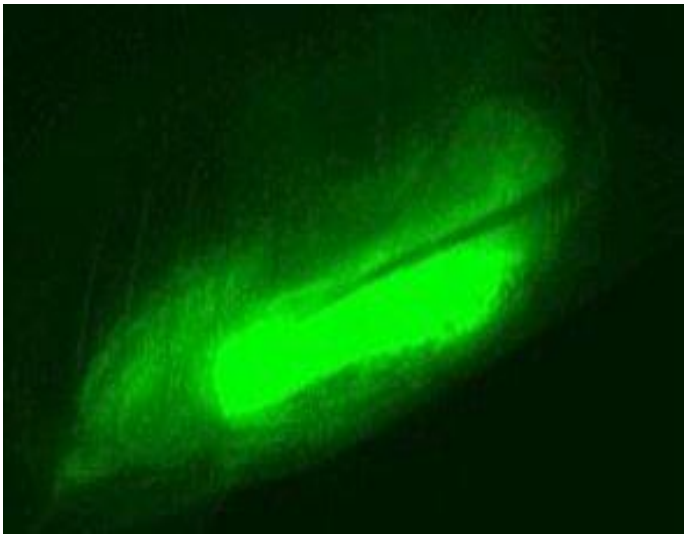

e)

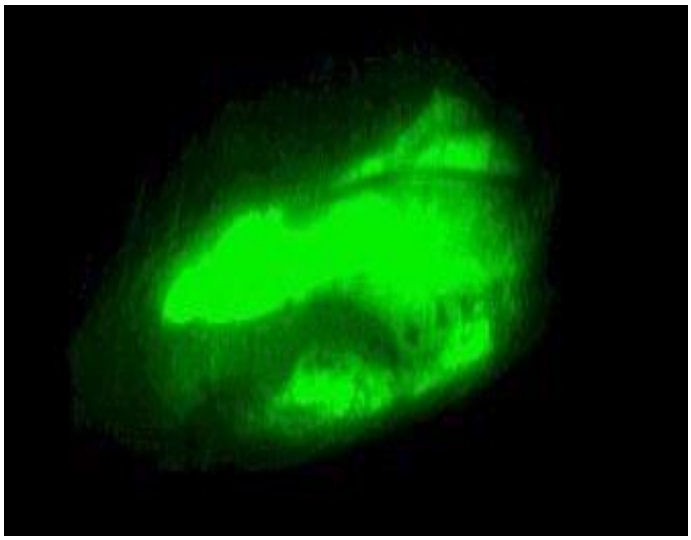

f)

g)

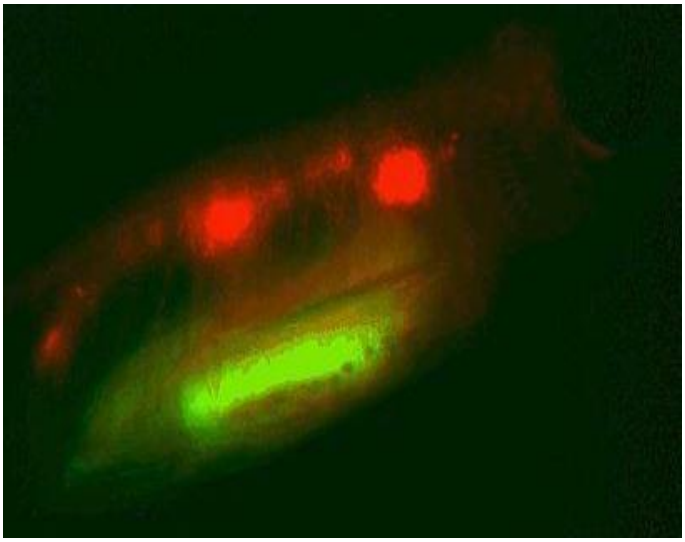

h)

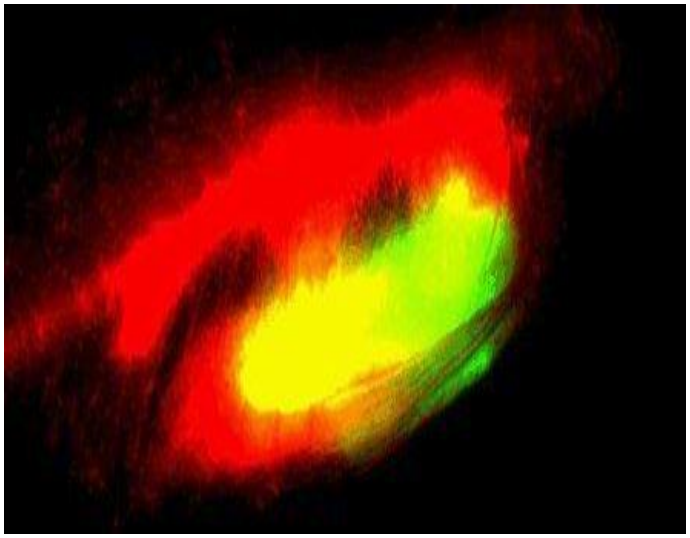

i)

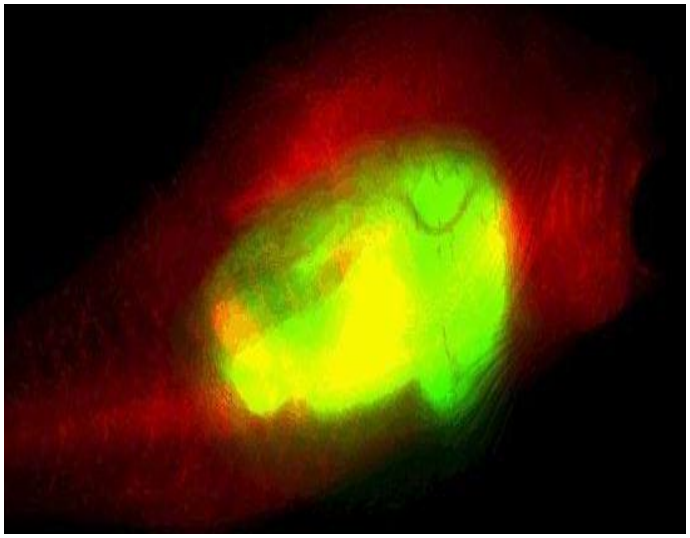

Figure IV: Images of the mCherry channel for fish 1 at a) imaging round I, b) imaging round II and c) imaging round III, images of the GFP channel for fish 1 at d) imaging round I, e) imaging round II and f) imaging round III and images of both mCherry and GFP together g) imaging round I, h) imaging round II and i) imaging round III. The fish was in approximately the same position in all images used and only the relevant areas of interest were included, with the area zoomed into kept the same size for all images so direct size comparisons are possible.

It is clear from the images including both tumour size and vasculature that there was a significant increase in tumour size as the experiment progressed, to the extent that slower tumour progression may be more desirable for comparative purposes as the GFP fluorescence (which also continually increased) became too bright to accommodate for mCherry fluorescence. From the mCherry channel images it seems as if fluorescence intensity increased in the region near the tumour, though closer inspection is necessary.

a)

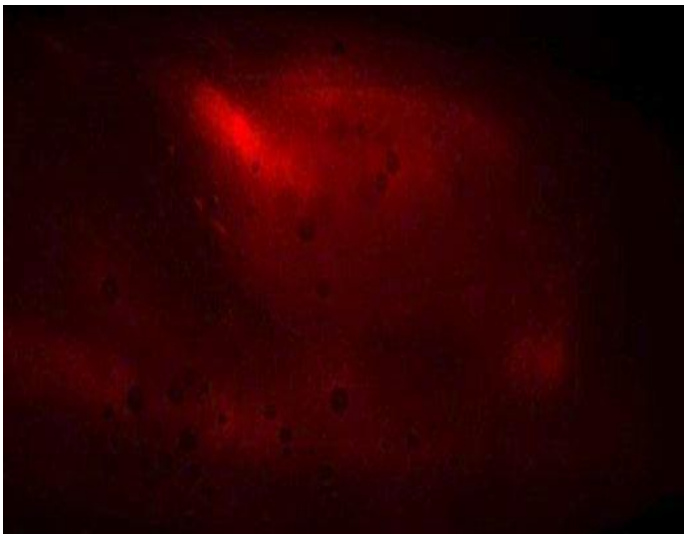

b)

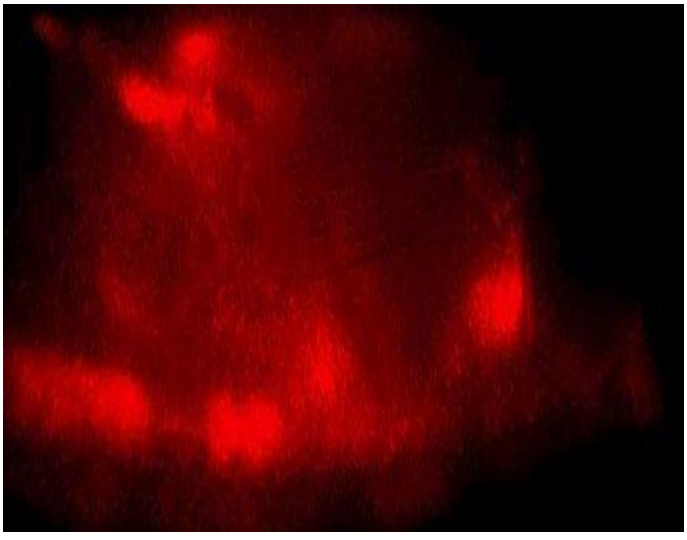

c)

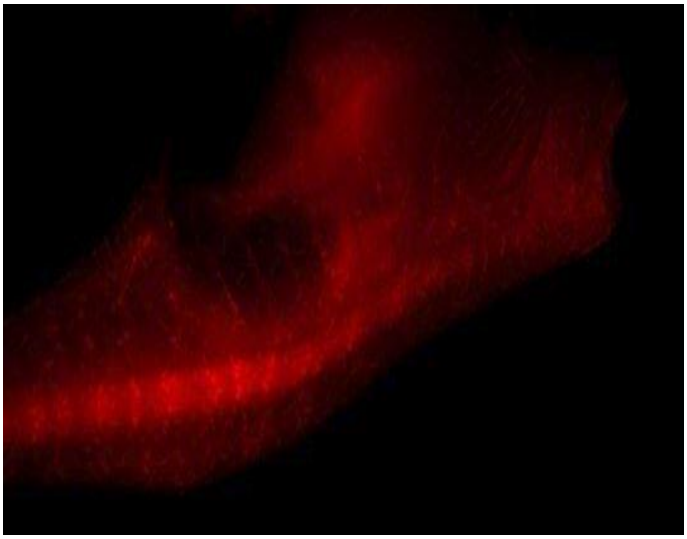

d)

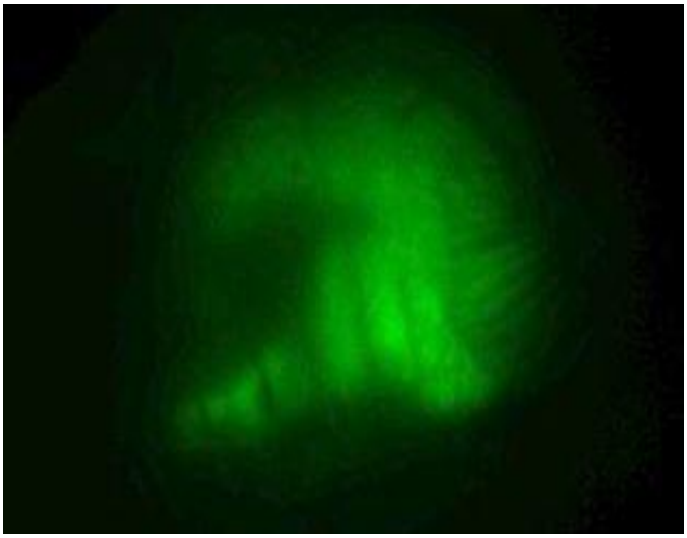

e)

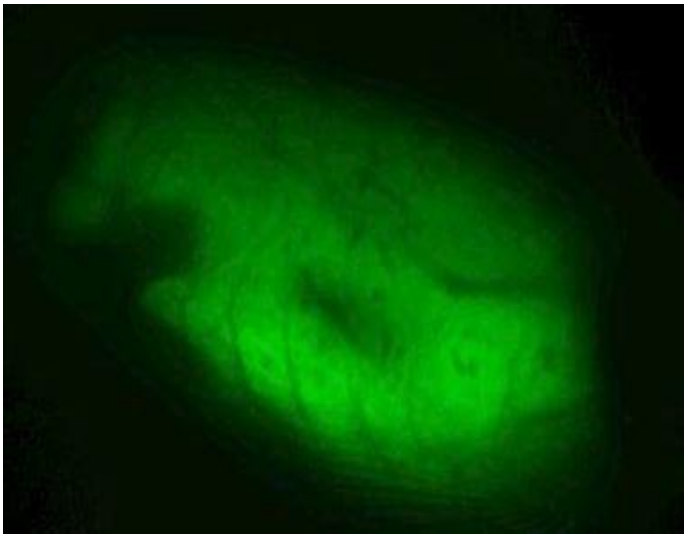

f)

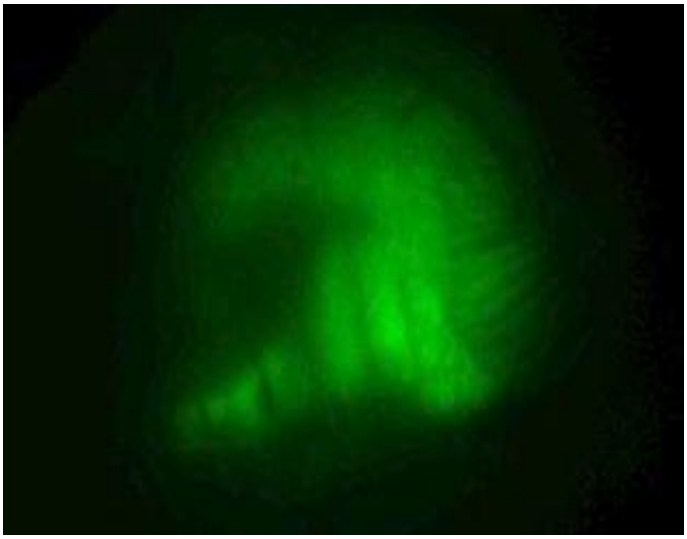

g)

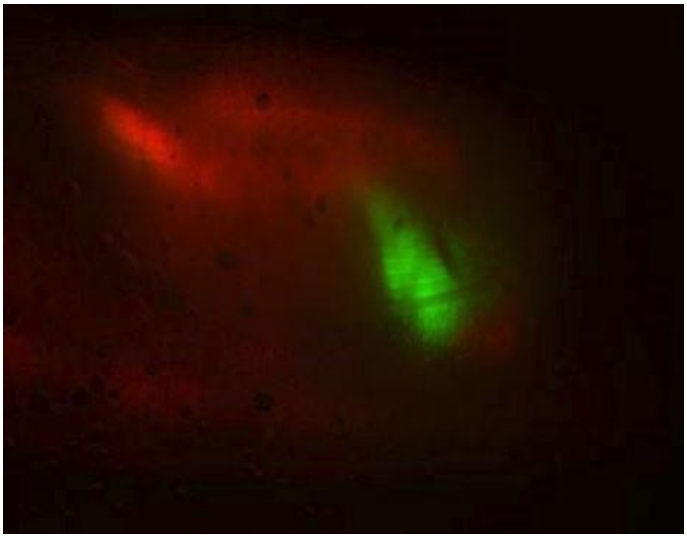

h)

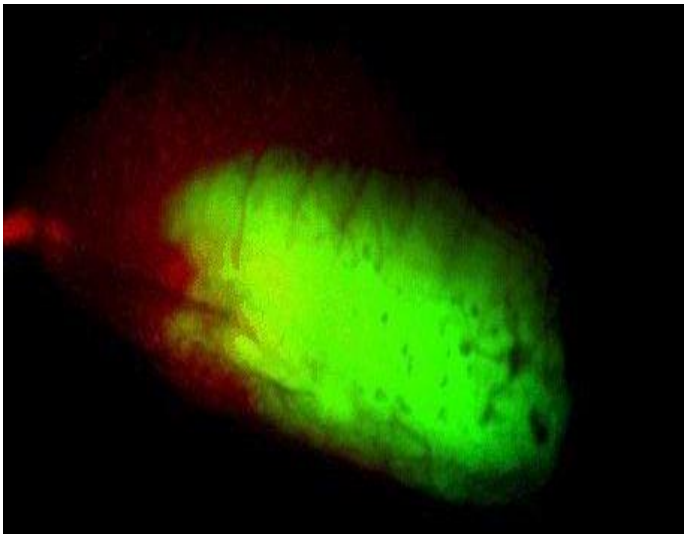

i)

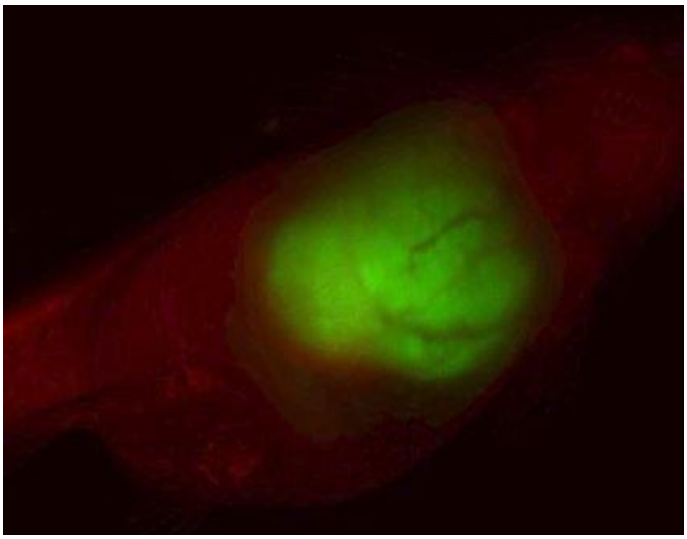

Figure V: Images of the mCherry channel for fish 6 at a) imaging round I, b) imaging round II and c) imaging round III, images of the GFP channel for fish 6 at d) imaging round I, e) imaging round II and f) imaging round III and images of both mCherry and GFP together g) imaging round I, h) imaging round II and i) imaging round III. The fish was in approximately the same position in all images used and only the relevant areas of interest were included, with the area zoomed into kept the same size for all images so direct size comparisons are possible.

Gifs of the image sequences for fish 6 are included in appendix IV. Once again significant tumour growth is evident, although by the last set of images the tumour seems to have slightly decreased in size as there appears to be less GFP fluorescence – this is may be the results of a large build-up of fluid surrounding the tumour which is evident from the image sequences included in appendix IV.

In comparison to images taken of zebrafish tumours using ultrasound biomicroscopy [Goessling *et al.*, 2008] or Magnetic Resonance Imaging [Kabli *et al.*, 2010], these OPT images are able to show the extent of tumour progression and vascularisation more precisely. The longitudinal study was unfortunately curtailed by the death of the fish, but the results even from only a few imaging rounds are encouraging enough to promote a longer term study.

Maximum Tolerated Dose of Doxycycline for zebrafish

In order to investigate the effect of doxycycline concentration on tumour progression and life expectancy of the zebrafish, it was decided to place six fish individually into separate tanks containing various doxycycline concentrations and to weigh them regularly to monitor tumour progression. The zebrafish selected were semi-pigmented heterozygous casper mutants and they were maintained in an identical manner to the previous description, with the exception of the varied level of doxycycline concentration. All zebrafish were born 68 days before the experiment started.

The zebrafish were initially weighed before being placed in water containing varying doxycycline concentrations, and were then weighed two, five, seven, nine and twelve days after the experiment commenced.

Fish marker	Doxycycline concentration (mg/L)	Weight at first weighing (mg)	Weight at second weighing (mg)	Weight at third weighing (mg)	Weight at fourth weighing (mg)	Weight at fifth weighing (mg)	Weight at sixth weighing (mg)
a	0	400	400	440	440	410	390
b	1.50	230	250	240	250	250	240
c	3.75	500	460	470	450	460	520
d	7.50	320	390	390	370	390	440
e	15.0	260	310	330	420	430	Deceased
f	75.0	400	Deceased	Deceased	Deceased	Deceased	Deceased

Table III: The weight in milligrams of the six fish chosen to investigate the effect of varying the concentration of doxycycline used to induce tumour growth. The fish were weighed at six separate time points.

Fish f died less than 24 hours after being placed into water containing a doxycycline concentration of 75 mg/L, almost certainly because of the high toxicity of the water. Fish e, whose doxycycline concentration was the same as the zebrafish previously used for imaging, demonstrated a significant increase in weight over the course of the experiment that was not strongly seen for the other fish (both fish c and d show large increases in weight at certain time points but for long periods their weight remained essentially static). This surge is seen most clearly between the third and fourth weighing's.

In addition to this fish e died approximately nine days after being introduced to the doxycycline containing water, which is comparable to the length of time taken to death for the zebrafish used for the longitudinal study. It is reasonable to hypothesise therefore that the maximum tolerated dose is somewhere between 7.50 and 15.0 mg/L and further tests in the future could be done to provide a more accurate estimate.

All surviving fish were imaged on the final day of the experiment to investigate the amount, if any, of tumour progression that had occurred, with figure V contains several relevant images. No GFP channel images were included for either fish a or b because there was no observable tumour formation (this of course would be expected for fish a, and it is possible that the concentration of doxycycline that fish b was exposed to was too small for significant tumour progression over the period of time the zebrafish were followed for). Significant light scattering in the mCherry channel images for the all fish prevented their inclusion – this provides a strong reason for this mutant not being used in future experiments.

a) b)

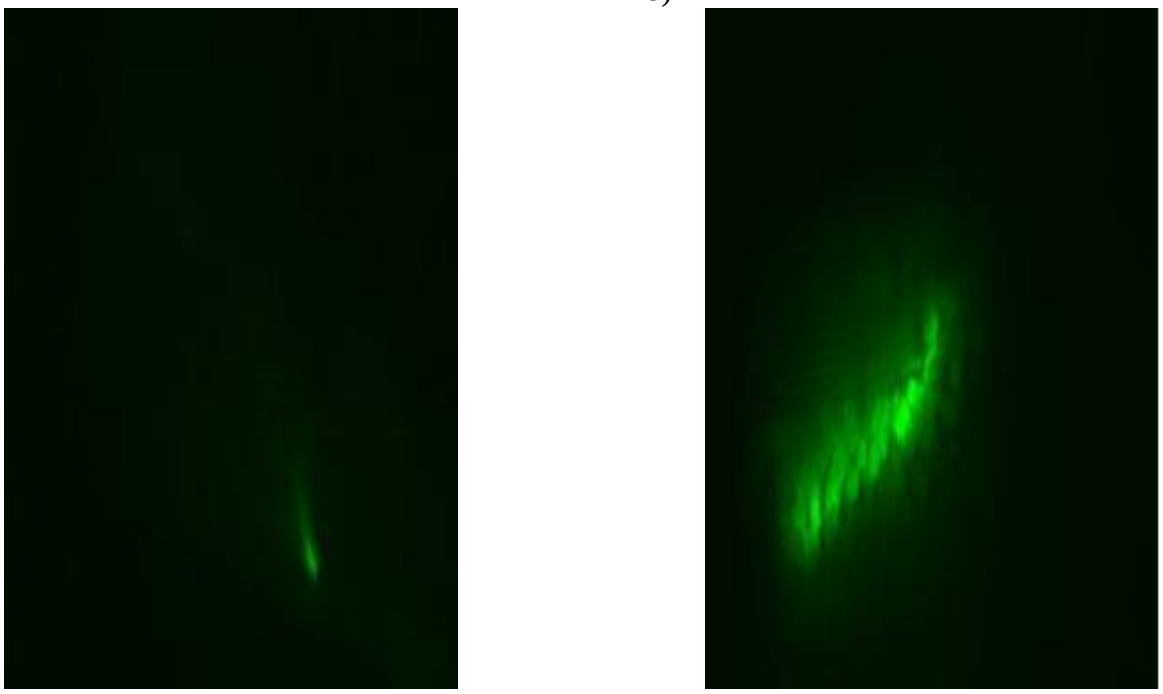

Figure VI: Single GFP channel images for a) fish c and b) fish d respectively. The level of zoom was kept the same for both fish so the comparative size of the tumours can be assessed and the entire fish is included in both images so that the comparative tumour size can be judged.

From the figure it is clear that even at half the standard doxycycline concentration significant tumour progression is possible, suggesting that for future longitudinal studies this, or a similar concentration, should be utilised because of the possible increased life expectancy and slower tumour growth. The results for fish c, which was introduced to water containing a quarter of the standard doxycycline concentration, indicated some level of tumour progression but possibly at too slow a rate to be of practical use.

Future improvements

Whilst the imaging techniques under consideration in this project are already capable of producing high quality results, there are a number of changes that could be explored in the future to see if possible improvements could be made.

For example, during the experiment a number of the zebrafish were lost due to extended times under anaesthesia. Refinement of the protocol therefore should be a priority if more longitudinal studies are to be done, especially for fish with significant tumour progression which may be at a greater risk of recovering from long term anaesthesia. The time of day at which the procedure occurs could also be standardised because of studies strongly implicating daily rhythms as being important in determining such factors as the recovery time and toxicity threshold for the zebrafish [Sánchez-Vázquez *et al.*, 2011].

The possibility of directly injecting the zebrafish with an anaesthetic, rather than introducing the fish to a solution containing tricaine, should also be considered as this would allow for a greater knowledge of exactly how much of the tricaine the zebrafish has absorbed [Kinkel *et al.*, 2010]. Larger fish could thus be given a more precise increased dose of tricaine which would hopefully reduce the number of fatalities (size being a significant factor in determining anaesthetic effectiveness [Rombough, 2007]). It is also important that the optimum doxycycline dosage is found to prevent premature zebrafish mortalities.

The constant development and refinement of models of cancer is essential if previous

advances in treatment are to further improved [Begley and Ellis, 2012]. This is particularly true for zebrafish models because of previous criticisms of murine models [Francia and Kerbel, 2010]. Given that approximately 90% of all cancer mortalities are due to metastasis [Brabletz, 2012] a complex zebrafish model of metastasis that apes human cancer and is able to allow metastatic cells to travel greater distances between tissues would be of great value, with some recent work being conducted in this direction [He *et al.*, 2012].

Another of the most sought after cancer models is a model of cancer cachexia. Cachexia involves the atrophy of host tissues as the tumour devours essential substances such as glucose and amino acids [Tisdale, 2001] and can have a serious impact on the host's quality of life and survival chances [Strasser and Bruera, 2002]. By pulsing the exposure of the zebrafish to doxycycline, rather than merely leaving them exposed to the antibiotic over a period of time, it is theorised that such a cancer model could be developed.

The two major areas of research for improving OPT are acquisition time reduction and increasing the image resolution.

It is currently typical for images to be taken at every 1° for a complete 360° rotation, which is relatively time consuming. This could be made faster by taking fewer pictures at larger angle spaces and then using an iterative model based on the acquired images to create the 'missing' images. Alternatively, using a multiple camera or mirror system seems to be a promising avenue of interest: the use of a dual-axis system of OPT has been shown to decrease image acquisition time and improve image resolution by using two orthogonal cameras with higher numerical apertures than previously used [Chen *et al.*, 2013]. Similarly a multi-mirror set-up comparable to already existing systems, such as the TCCAGE [OPTO Engineering, 2013], could help to increase the efficiency of image attainment.

Whilst OPT has been clearly demonstrated to be a reliable imaging technique there is on-going research into other areas of tomography, such as Diffuse Optical Tomography (DOT). Unlike OPT, which assumes that photons travel in a straight line from the light source to the detector through the sample, DOT allows for scattering to occur once the light enters the sample [Arridge, 1999] and as such could potentially provide a more accurate final representation. Although DOT is currently unable to produce as high quality images as OPT it does allow for investigation into the scattering and absorption parameters of the sample being imaged and recent improvements in artefact reduction and reconstruction time are significant [Heiskala *et al.*, 2012].

Acknowledgements

I would like to thank both of my supervisors for their invaluable help and guidance throughout the project. I would also like to acknowledge the assistance of Jia Chan from the Division of Biosciences at University College London, Professor Simon Arridge from the Department of Computer Science at University College London, and Professor Paul French, Dr. James McGinty, Lingling Chen and Sunil Kumar from the Department of Physics at Imperial College London.

References

Allen, J.P. and Neely, M.N. (2010) 'Trolling for the ideal host: zebrafish take the bait' *Future Microbiol.* 2010 April; 5(4): 563-569.

Amatruda, J.F., Shepard, J.L., Stern, H.M. and Zon, L.I. (2002) 'Zebrafish as a cancer model system' *Cancer Cell* 1:229-31.

Aoki, K., Kiyokawa, E., Nakamura, T. and Matsuda, M. (2008) 'Visualization of growth signal transduction cascades in living cells with genetically encoded probes based on Förster resonance energy transfer' *Phil. Trans. R. Soc. B* June 2008; 363(1500); 2143-2151.

Arridge, S.R. (1999) "Optical tomography in medical imaging" *Inverse Problems* 1999; 15:41–93.

Bassi, A., Fieramonti, L., D'Andrea, C., Mione, M. and Valentini, G. (2011) *'In vivo* label-free three-dimensional imaging of zebrafish vasculature with Optical Projection Tomography' *J. Biomed. Opt*. 16(10), 100502.

Begley, C.G. and Ellis, L.M. (2012) 'Drug development: Raise standards for preclinical cancer research' *Nature* 2012; 483; 531-533.

Brabletz, T. (2012) 'EMT and MET in Metastasis: Where Are the Cancer Stem Cells?' *Cancer Cell* 2012; 22(6); 699-701.

Chang, C.W., Sud, D. and Mycek, M.A. (2007) 'Fluorescence-lifetime Imaging Microscopy' *Methods in Cell Biology* 2007; 81: 495-524.

Cheddad, A., Svensson, C., Sharpe, J., Georgsson, F. and Ahlgrel, U. (2012) 'Image Processing Assisted Algorithms for Optical Projection Tomography' *IEE Trans Med Imaging* Jan 2012; 31(1).

Chen, L., Andrews, N., Kumar, S., Frankel, P., McGinty, J., and French, P.M.W. (2013) 'Simultaneous angular multiplexing optical projection tomography at shifted focal planes' *Optics Letters* 2013; 38(6): 851-853.

Davison, J.M., Park, S.W., Rhee, J.M. and Leach, S.D. (2008) 'Characterization of Kras-Mediated pancreatic tumorigenesis in zebrafish' *Methods in Enzymology* 438.

Feitsma, H. and Cuppen, E. (2008) 'Zebrafish as a cancer model' *Mol. Cancer Res.* 2008; 6(5).

Fieramonti, L., Bassi, A., Foglia, E.A., Pistochi, A., D'Andrea, C., Valenti, G., Cubeddu, R., De Silvestri, S., Cerullo, G. and Cotelli, F. (2012) 'Time-Gated Optical Projection Tomography Allows Visualization of Adult Zebrafish Internal Structures' *PLoS ONE* 2012; 7(11): e50744.

Francia, G. and Kerbel, R.S. (2010) 'Raising the bar for cancer therapy models' *Nature Biotechnology* 2010; 28; 561-562.

Goessling, W., North, T.E. and Zon, L.I. (2007) 'Ultrasound biomicroscopy permits *in vivo* characterization of zebrafish liver tumors' *Nature Methods* 2007; 4: 551 – 553.

Hall, A. (2005) 'Rho GTPases and the control of cell behaviour' *Biochem Soc Trans* Nov 2005; 33(5): 891-5.

Hanahan, D. and Weinberg, R.A. (2011) 'Hallmarks of Cancer: The Next Generation' *Cell* 2011; 144: 646 – 674.

He, S., Lamers, G.E.M., Beenakker, J.W.M., Cui, C., Ghotra, V.P.S., Danen, E.H.J., Meijer, A.H., Spaink, H.P. and Snaar-Jagalska, B.E. (2012) 'Neutrophil-mediated experimental metastasis is enhanced by VEGFR inhibition in a zebrafish xenograft model' *J Pathol* 2012; 227: 431–445.

Heiskala, J., Kolehmainen, V., Tarvainen, T., Kaipio, J.P. and Arridge, S.R. (2012) 'Approximation error method can reduce artifacts due to scalp blood flow in optical brain activation imaging' *J. Biomed. Opt.*; 17(9): 096012.

Huang, W.C., Hsieh, Y.S., Chen, I.H., Wang, C.H., Chang, H.W., Yang, C.C., Ku, T.K., Yeh, S.R. and Chuang, Y.J. (2010) 'Combined Use of MS-222 (Tricaine) and Isoflurane Extends Anesthesia Time and Minimizes Cardiac Rhythm Side Effects in Adult Zebrafish' *Zebrafish* 2010; 7(3).

Invitrogen™ (2010) 'pDisplay™ Vector for expression of proteins on the surface of mammalian cells'. Available at http://tools.invitrogen.com/content/sfs/manuals/pdisplay_man.pdf
Last accessed 30th April 2013.

Invitrogen™ (2010a). 'pcDNA™3.1(+) pcDNA™3.1(–) ' Available at
http://tools.invitrogen.com/content/sfs/manuals/pcdna3_1_man.pdf
Last accessed 30th April 2013.

Invitrogen (2012) 'Lipofectamine® 2000 Reagent' Available at
http://tools.invitrogen.com/content/sfs/manuals/lipofectamine2000_man.pdf?ICID=cvc-lipofectamine-c2m2 Last accessed 30h April 2013.

Ishizawar, R. and Parsons, S.J. (2004). 'c-Src and cooperating partners in human cancer' *Cancer Cell* 2004; 6:209–14.

Kabli, S., He, S., Spaink, H.S., Hurlstone, A., Jagalska, E.S., De Groot, H.J.M. and Alia, A. (2010) '*In Vivo* Magnetic Resonance Imaging to Detect Malignant Melanoma in Adult Zebrafish' Zebrafish 2010; 7(2): 143-148.

Kak, A. C., and Slaney, M. (1988) 'Principles of Computerized Tomographic Imaging' New York, NY, IEEE Press, 1988.

Kinkel, M.D., Eames, S.C., Philipson, L.H. and Prince, V.E. (2010) 'Intraperitoneal Injection into Adult Zebrafish' *J. Vis. Exp.* 2010 (42), e212610.3791/2126.

Langheinrich, U. (2003) 'Zebrafish: a new model on the pharmaceutical catwalk'. *Bioessays* 2003; 25(9): 904–912.

Li, Z., Huang, X., Zhan, H., Zeng, Z., Li, C., Spitsbergen, J.M. Meierjohann, S., Scharti, M. and Gong, Z. (2012) 'Inducible and repressable oncogene-addicted hepatocellular carcinoma in Tet-on *xmrk* transgenic zebrafish' *J Hep* 2012; 56(2): 419-425.

Li, Z., Zheng, W., Wang, Z., Zeng, Z., Zhan, H., Li, C., Zhou, L., Yan, C., Spitsbergen, J.M. and Gong, Z. (2012a) 'A transgenic zebrafish liver tumor model with inducible *Myc* expression reveals conserved Myc signatures with mammalian liver tumors' *Dis Model Mech* 2012; 6(2): 414-23.

Liu, S. and Leach, S.D. (2011) 'Zebrafish models for cancer' *Annu. Rev. Pathol. Mech. Dis.* 2011;

6:71-93.

McGinty, J., Taylor, H.B., Chen, L., Bugeon, L., Lamb, J.R., Dallman, M.J. and French, P.M.W. (2011) '*In vivo* fluorescence lifetime optical projection tomography' *Biomedical Optics Express* May 2011: 2(5): 1340-50.

Nguyen, A.T., Emelyanov, A., Koh, C.H.V., Spitsbergen, J.M., Parinov, S. and Gong, Z. (2012) 'An inducible kras^{V12} transgenic zebrafish model for liver tumorigenesis and chemical drug screening' *Dis Mod Mech* Jan 2012; 5: 63-72.

Nyalendo C, Michaud M, Beaulieu E, Roghi, C., Murphy, G., Gingras, D. and Beliveau, R. (2007) 'Src-dependent phosphorylation of membrane type I matrix metalloproteinase on cytoplasmic tyrosine 573: role in endothelial and tumor cell migration' *J Biol Chem* 2007; 282: 15690–9.

OPTO Engineering (2013) 'Multiple Side Imaging And Measurement At 90°' Available at http://www.opto-engineering.com/brochure/TCCAGE.pdf Last accessed 30th April 2013.

Ouyang, M., Sun, J., Chien, S. and Wang, Y. (2008) 'Determination of hierarchical relationship of Src and Rac at subcellular locations with FRET biosensors' *Proc Natl Acad Sci U S A* September 2008; 105(38): 14353–14358.

Ouyang, M., Lu, S., Li, X.-L., Xu, J., Seong, J., Giepman, B.N.G., Shyy, J.Y.-J., Weiss, S.J., and Wang, Y. (2008a) 'Visualization of Polarized Membrane Type 1 Matrix Metalloproteinase Activity in Live Cells by Fluorescence Resonance Energy Transfer Imaging' *J Bio Chem* 2008;283(25): 17740-48.

Ouyang, M., Huang, H., Shaner, N.C., Remacle, A.G., Shiryaev, S.A., Strongin, A.Y., Tsien, R.Y. and Wang, Y. (2010). 'Simultaneous Visualization of Protumorigenic Src and MT1-MMP Activities with Fluorescence Resonance Energy Transfer' *Cancer Res.* March 2010: 70(6).

Richards, M.A., Stockton, D., Babb, P. and Coleman, M.P. (2000). 'How many deaths have been avoided through improvements in cancer survival?' *BMJ* 2000; 320: 895–8.

Roche (2013) 'FuGene HD® Transfection Reagent; Available at https://cssportal.roche.com/LFR_PublicDocs/ras/04709705001_en_13.pdf Last accessed 30th April 2013.

Rombough, P.J. (2007) 'Ontogenetic changes in the toxicity and efficacy of the anaesthetic MS222 (tricaine methanesulfonate) in zebrafish (*Danio rerio*) larvae' *Comp. Biochem. Physiol. A Mol. Integr. Physiol* 2007; 148:463–469.

Sánchez-Vázquez, F.J., Terry, M.I., Felizardo, V.O. and Vera, L.M. 'Daily Rhythms of Toxicity and Effectiveness of Anesthetics (MS222 and Eugenol) in Zebrafish (*Danio Rerio*)' *Chronobiology International* 2011; 28(2): 109–117

Santoriello, C. and Zon, L.I. (2012) 'Hooked! Modeling human disease in zebrafish' *J Clin Invest.* 2012; 122(7): 2337–2343.

Seiki, M. (2003). 'Membrane-type 1 matrix metalloproteinase: a key enzyme for tumor invasion' *Cancer Lett.* 2003 May 8; 194(1): 1-11.

Seiki, M., Mori, H. Kajita, M., Uekita, T. and Itoh, Y. (2003). 'Membrane-type 1 matrix metalloproteinase and cell migration' *Biochem Soc. Symp*. 2003; 70: 253-62.

Sharpe, J. (2004) 'Optical projection tomography' *Annu. Rev. Biomed. Eng*. 2004. 6:209–28.

Sharpe, J., Ahlgren, U., Perry, P., Hill, B., Ross, A., Hecksher-Sorenson, J., Baldock, R. and Davidson, D. (2002). 'Optical Projection Tomography as a tool for 3D microscopy and gene expression studies' *Science* 296 541.

Spitsbergen, J. (2007) 'Imaging neoplasia in fish' *Nature Methods* July 2007; 4(7): 548-549.

Stoletov, K. and Klemke, R. (2008) 'Catch of the day: zebrafish as a human cancer model' *Oncogene* 2008 27, 4509-4520.

Strasser, F. and Bruera, E.D. (2002) 'Update on anorexia and cachexia' *Hematol Oncol Clin North Am.* 2002; 16: 589–617.

Tisdale, M.J. (2001) 'Cancer anorexia and cachexia' *Nutrition* 2001 May; 17(5): 438-42.

Verveer, P.J. and Bastiaens, P.I.H. (2007). 'Quantitative microscopy and systems biology: seeing the whole picture' *Histochem Cell Biol.* 2007; 130: 833-843.

Wilson, J.M., Bunte, R.M., and Carty, A.J. (2009) 'Evaluation of Rapid Cooling and Tricaine Methanesulfonate (MS222) as Methods of Euthanasia in Zebrafish (*Danio rerio*)' *JAALAS* 2009; 48(6): 785–789.

World Health Organization 'Cancer Factsheet No. 297' Available at: http://www.who.int/mediacentre/factsheets/fs297/en/ Last accessed 30th April 2013.

Yancik, R. and Ries, L.A. (2004). 'Cancer in older persons: an international issue in an aging world' *Semin Oncol*. 2004 Apr; 31(2): 128-36.

Zheng, J. (2006). 'Spectroscopy-Based Quantitative Fluorescence Resonance Energy Transfer Analysis'. In Stockand, J. D.; Shapiro, M. S. *Ion Channels: Methods and Protocols*. Methods in Molecular Biology, Volume 337. Totowa, NJ: Humana Press. pp. 65–77.

Zhu, S., Dong, D., Birk, U.J., Rieckher, M., Tavernarakis, N., Qu, X., Liang, J., Tian, J. and Ripoll, J. (2012) 'Automated motion correction for in vivo optical projection tomography' *IEE Trans Med Imaging* 2012 Jul; 31(7): 1358-71.

Appendices

Appendix I: A visual representation of the mechanism of action of the Src biosensor

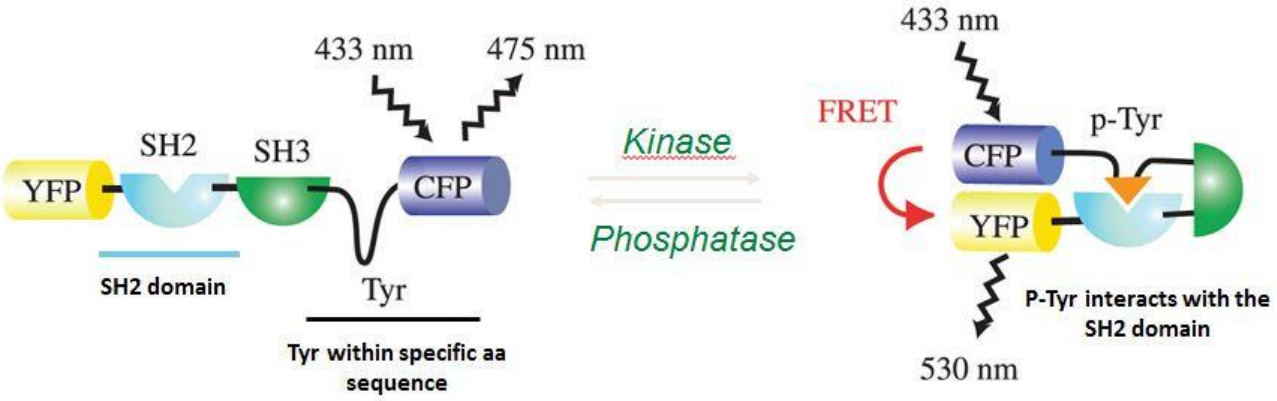

The above image, modified from Aoki *et al.*, 2008, displays how the biosensor contorts in the presence of the appropriate kinase and so enables FRET to occur. The biosensor returns to its original position afterwards.

Appendix II: Nucleotide and protein sequences for the MT1-MMP and Src biosensors

MT1-MMP results

Nucleotide sequence

ATGTCTAAAGGTGAAGAATTATTCACTGGTGTTGTCCCAATTTTGGTTGAATTAGATGGT
GATGTTAATGGTCACAAATTTTCTGTCTCCGGTGAAGGTGAAGGTGATGCTACGTACGGT
AAATTGACCTTAAAATTACTCTGTACTACTGGTAAATTGCCAGTTCCATGGCCAACCTTA
GTCACTACTTTAGGTTATGGTGTTCAATGTTTTGCTAGATACCCAGATCATATGAAACAAC
ATGACTTTTTCAAGTCTGCCATGCCAGAAGGTTATGTTCAAGAAAGAACTATTTTTTTCA
AAGATGACGGTAACTACAAGACCAGAGCTGAAGTCAAGTTTGAAGGTGATACCTTAGTT
AATAGAATCGAATTAAAAGGTATTGATTTTAAAGAAGATGGTAACATTTTAGGTCACAAA
TTGGAATACAACTATAACTCTCACAATGTTTACATCACTGCTGACAAACAAAAGAATGGT
ATCAAAGCTAACTTCAAAATTAGACACAACATTGAAGATGGTGGTGTTCAATTAGCTGA
CCATTATCAACAAAATACTCCAATTGGTGATGGTCCAGTCTTGTTACCAGACAACCATTA
CTTATCCTATCAATCTGCCTTATTCAAAGATCCAAACGAAAAGAGAGACCACATGGTCTT
GTTAGAATTTTTGACTGCTGCTGGTATTACCGAGGGTATGAATGAATTGTACAAAGAGCT
CTGCCCCAAGGAGAGCTGCAACCTGTTTGTGCTGAAGGACATGGTGAGCAAGGGCGAG
GAGCTGTTCACCGGGGTGGTGCCCATCCTGGTCGAGCTGGACGGCGACGTAAACGGCC
ACAGGTTCAGCGTGTCCGGCGAGGGCGAGGGCGATGCCACCTACGGCAAGCTGACCCT
GAAGTTCATCTGCACCACCGGCAAGCTGCCCGTGCCCTGGCCCACCCTCGTGACCACCC
TGACCTGGGGCGTGCAGTGCTTCAGCCGCTACCCCGACCACATGAAGCAGCACGACTTC
TTCAAGTCCGCCATGCCCGAAGGCTACGTCCAGGAGCGTACCATCTTCTTCAAGGACGA
CGGCAACTACAAGACCCGCGCCGAGGTGAAGTTCGAGGGCGACACCCTGGTGAACCGC
ATCGAGCTGAAGGGCATCGACTTCAAGGAGGACGGCAACATCCTGGGGCACAAGCTGG
AGTACAACTACATCAGCCACAACGTCTATATCACCGCCGACAAGCAGAAGAACGGCATC
AAGGCCCACTTCAAGATCCGCCACAACATCGAGGACGGCAGCGTGCAGCTCGCCGACC
ACTACCAGCAGAACACCCCCATCGGCGACGGCCCCGTGCTGCTGCCCGACAACCACTA
CCTGAGCACCCAGTCCGCCCTGAGCAAAGACCCCAACGAGAAGCGCGATCACATGGTC
CTGCTGGAGTTCGTGACCGCCGCCCTGCAGGTCGACGAACAAAAACTCATCTCAGAAG
AGGATCTGAATGCTGTGGGCCAGGACACGCAGGAGGTCATCGTGGTGCCACACTCCTTG

CCCTTTAAGGTGGTGGTGATCTCAGCCATCCTGGCCCTGGTGGTGCTCACCATCATCTCC
CTTATCATCCTCATC

Protein sequence

MSKGEELFTGVVPILVELDGDVNGHKFSVSGEGEGDATYGKLTLKLLCTTGKLPVPWPTL
VTTLGYGVQCFARYPDHMKQHDFFKSAMPEGYVQERTIFFKDDGNYKTRAEVKFEGDTLV
NRIELKGIDFKEDGNILGHKLEYNYNSHNVYITADKQKNGIKANFKIRHNIEDGGVQLAD
HYQQNTPIGDGPVLLPDNHYLSYQSALFKDPNEKRDHMVLLEFLTAAGITEGMNELYKEL
CPKESCNLFVLKDMVSKGEELFTGVVPILVELDGDVNGHRFSVSGEGEGDATYGKLTLKF
ICTTGKLPVPWPTLVTTLTWGVQCFSRYPDHMKQHDFFKSAMPEGYVQERTIFFKDDGNY
KTRAEVKFEGDTLVNRIELKGIDFKEDGNILGHKLEYNYISHNVYITADKQKNGIKAHFK
IRHNIEDGSVQLADHYQQNTPIGDGPVLLPDNHYLSTQSALSKDPNEKRDHMVLLEFVTA
ALQVDEQKLISEEDLNAVGQDTQEVIVVPHSLPFKVVVISAILALVVLTIISLIILI

Biosensor outline

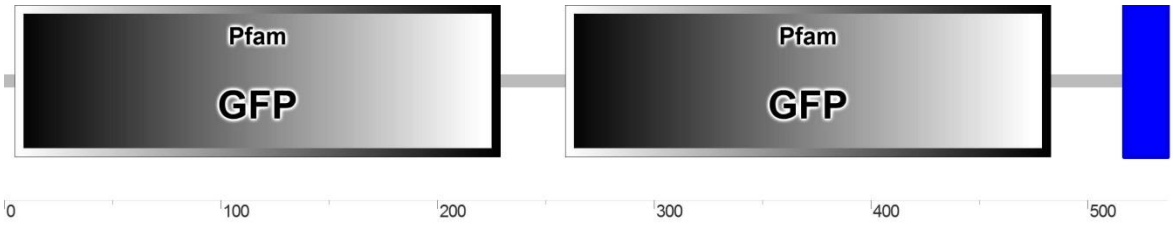

MT1-MMP contains both mCherry and mOrange2 fluorophores, and a transmembrane domain as illustrated above (the Blast result is GFP for both fluorophores because of the close similarity of the nucleotide sequences but mCherry and mOrange2 had equivalent P values to GFP).

Src results

Nucleotide sequence

CCTCTAGATGCATGCTCGAGCGGCCGCCAGTGTGATGGATATCTGCAGAATTCTTACATG
ATCACGCACTTGGTCTTGCTCTTCTTCTTCTTCTTCTTTTTGTACAATTCATTCATACCCTC
GGTAATACCAGCAGCAGTCAAAAATTCTAACAAGACCATGTGGTCTCTCTTTTCGTTTGG
ATCTTTGAATAAGGCAGATTGATAGGATAAGTAATGGTTGTCTGGTAACAAGACTGGACC
ATCACCAATTGGAGTATTTTGTTGATAATGGTCAGCTAATTGAACACCACCATCTTCAATG
TTGTGTCTAATTTTGAAGTTAGCTTTGATACCATTCTTTTGTTTGTCAGCAGTGATGTAAA
CATTGTGAGAGTTATAGTTGTATTCCAATTTGTGACCTAAAATGTTACCATCTTCTTTAAA
ATCAATACCTTTTAATTCGATTCTATTAACTAAGGTATCACCTTCAAACTTGACTTCAGCT
CTGGTCTTGTAGTTACCGTCATCTTTGAAAAAAATAGTTCTTTCTTGAACATAACCTTCTG
GCATGGCAGACTTGAAAAAGTCATGTTGTTTCATATGATCTGGGTATCTAGCAAAACATT
GAACACCATAACCTAAAGTAGTGACTAAGGTTGGCCATGGAACTGGCAATTTACCAGTA
GTACAGAGTAATTTTAAGGTCAATTTACCGTACGTAGCATCACCTTCACCTTCACCGGAG
ACAGAAAATTTGTGACCATTAACATCACCATCTAATTGAACACCATAACCTAAAGTAGTG
ACTAAGGTTGGCCATGGAACTGGCAATTTACCAGTAGTACAGAGTAATTTTAAGGTCAAT
TTACCGTACGTAGCATCACCTTCACCTTCACCGGAGACAGAAAATTTGTGACCATTAACA
TCACCATCTAATTCAACCAAAATTGGGACAACACCAGTGAATAATTCTTCACCTTTAGAG
AGCTCCCCCTGTAGGTGGACGTAGTCATAGTCCTCCATCCAAGAACCCTCACCAGAACC
CGGCTTCCCAGATCCAGATGTAGACCCACAGACGTTAGTCAGGCGGTGGCACAAGCCAT

CAGCATGTTTGGAGTAGTAGGCCACCAGCTGCTGCAGGCTGCTGAACTGTGTGCGTGAG
GTGATGTAGAAGCCGCCGCTGTCCAGCTTGCGGATCTTGTAGTGCTTCACATTGAGCCCC
TTGGCGTTGTCAAAGTCAGAAACGGAGAGGCAATAGGCACCTTTTGTCGTCTCGCTCTC
CCGGACCAAGAAGGTTCCCCGGGGGTTTTCGGGGTTGAGCAGCAGCCGCTCGGACTCC
CGACGAGTGATCTTCCCAAAATACCAATGCATGCGGGCGGCGGTCACGAACTCCAGCAG
GACCATGTGATCGCGCTTCTCGTTGGGGTCTTTGCTCAGGGCGGACTGGGTGCTCAGGT
AGTGGTTGTCGGGCAGCAGCACGGGGCCGTCGCCGATGGGGGTGTTCTGCTGGTAGTG
GTCGGCGAGCTGCACGCTGCCGTCCTCGATGTTGTGGCGGATCTTGAAGTGGGCCTTGA
TGCCGTTCTTCTGCTTGTCGGCGGTGATATAGACGTTGTGGCTGATGTAGTTGTACTCCA
GCTTGTGCCCCAGGATGTTGCCGTCCTCCTTGAAGTCGATGCCCTTCAGCTCGATGCGGT
TCACCAGGGTGTCGCCCTCGAACTTCACCTCGGCGCGGGTCTTGTAGTTGCCGTCGTCC
TTGAAGAAGATGGTACGCTCCTGGACGTAGCCTTCGGGCATGGCGGACTTGAAGAAGTC
GTGCTGCTTCATGTGGTCGGGGTAGCGGC

Protein sequence

MSKGEELFTGVVPILVELDGDVNGHKFSVSGEGEGDATYGKLTLKLLCTTGKLPVPWPTLV
TTLGYGVQCFARYPDHMKQHDFFKSAMPEGYVQERTIFFKDDGNYKTRAEVKFEGDTLVN
RIELKGIDFKEDGNILGHKLEYNYNSHNVYITADKQKNGIKANFKIRHNIEDGGVQLADHY
QQNTPIGDGPVLLPDNHYLSYQSALFKDPNEKRDHMVLLEFLTAAGITEGMNELYKELCPK
ESCNLFVLKDMVSKGEELFTGVVPILVELDGDVNGHRFSVSGEGEGDATYGKLTLKFICTT
GKLPVPWPTLVTTLTWGVQCFSRYPDHMKQHDFFKSAMPEGYVQERTIFFKDDGNYKTRA
EVK

Biosensor outline

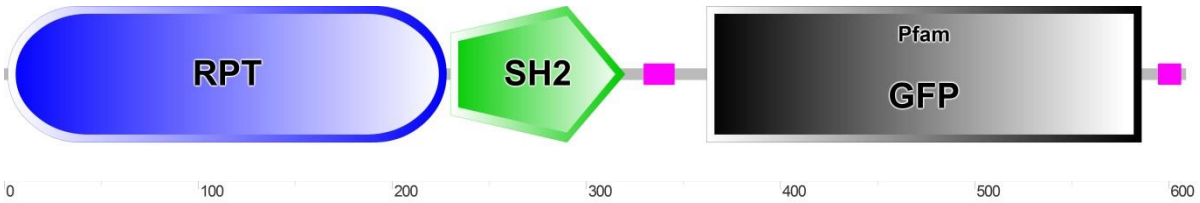

Src contains both ECFP and Citrine fluorophores, and a SH2 domain as illustrated above (the Blast result is GFP for both fluorophores because of the close similarity of the nucleotide sequences but ECFP and Citrine had equivalent P values to GFP).

Appendix III: Gifs of the image sequences for fish 1 of the mCherry channel at a) imaging round I, b) imaging round II and c) imaging round III, the image sequences of the GFP channel at d) imaging round I, e) imaging round II and f) imaging round III and both channels together at g) imaging round I, h) imaging round II and i) imaging round III

Appendix IV: Gifs of the image sequences for fish 6 of the mCherry channel at a) imaging round I, b) imaging round II and c) imaging round III, the image sequences of the GFP channel at d) imaging round I, e) imaging round II and f) imaging round III and both channels together at g) imaging round I, h) imaging round II and i) imaging round III